Exact Coupling Threshold for Structural Transition Reveals Diversified Behaviors in Interconnected Networks

Faryad Darabi Sahneh,[1] Caterina Scoglio,[1] and Piet Van Mieghem[2]

[1]*Electrical and Computer Engineering Department, Kansas State University*
[2]*Faculty of Electrical Engineering, Mathematics, and Computer Science, Delft University of Technology, Delft, The Netherlands*

An interconnected network features a structural transition between two regimes [1]: one where the network components are structurally distinguishable and one where the interconnected network functions as a whole. Our exact solution for the coupling threshold uncovers network topologies with unexpected behaviors. Specifically, we show conditions that superdiffusion, introduced in [2], can occur despite the network components functioning distinctly. Moreover, we find that components of certain interconnected network topologies are indistinguishable despite very weak coupling between them.

Several natural and human-made networks—such as power grids controlled by communications networks, contact networks of human and animal populations for transmission of zoonotic diseases, and transportation networks consisting of multiple modes (road, flights, railroads, etc.)—cannot be represented by simple graphs and have led [3] to the introduction of interdependent, interconnected, and multilayer networks in network science [4, 5]. Interconnected networks are mathematical representations of systems where two or more simple networks, possibly with different functionalities, are coupled to each other. The omnipresence of interconnected networks has spurred a variety of research [6–9], with particular interest in dynamical processes such as percolation [10, 11], epidemic spreading [12–15], and diffusion [2, 16].

Recently, Radicchi and Arenas [1], and Gomez *et al.* [2] proposed a stylized interconnected network [17], consisting of two connected networks, G_A and G_B, each of size N, with one-to-one interconnection, as sketched in Fig. 1, where the interconnection strength between the layers is parametrized by a coupling weight $p > 0$.

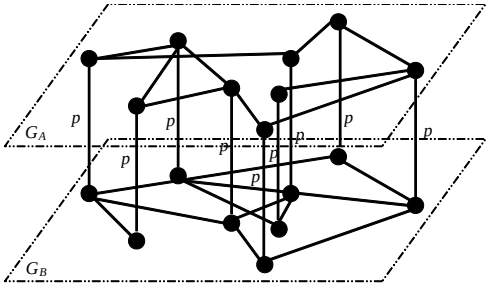

FIG. 1. One-to-one interconnection of two networks G_A and G_B, where the coupling weight is $p > 0$.

Radicchi and Arenas [1] demonstrated the existence of a *structural transition* point p^*. Depending on the coupling weight p between the two networks, the collective interconnected network can function in two regimes: *if $p < p^*$, the two networks are structurally distinguishable; whereas if $p > p^*$, they behave as a whole*.

While studying diffusion processes on the same type of interconnected network in Fig. 1, Gomez *et al.* [2] observed *superdiffusion*: for sufficiently large p, the *diffusion in the interconnected network takes place faster than in either of the networks separately*. Superdiffusion arises due to the synergistic effect of the network interconnection and exemplifies a characteristic phenomenon in interconnected networks. Placement of the introduction point of superdiffusion with respect to the critical point p^* is missing in the literature.

Whereas the existence of a critical transition p^* was reported in [1], here, we determine the exact coupling threshold p^*. Our exact solution illuminates the role of each individual network component and their combined configuration on the structural transition phenomena and uncovers unexpected behaviors. Specifically, we show structural transition is not a necessary condition for achieving superdiffusion. Indeed, superdiffusion can be achieved for a coupling weight p even below the structural transition threshold p^*, which is surprising because, intuitively, synergy is not expected if the network components are functioning distinctly. Moreover, we observe that the structural transition disappears when one of the network components has vanishing algebraic connectivity [18–20], as is the case for a class of scale-free networks. Therefore, components of such interconnected network topologies become indistinguishable despite very weak coupling between them.

Spectral analysis plays a key role in understanding interconnected networks. Hernandez *et al.* [21] found the complete spectra of interconnected networks with identical components. Sole-Ribalta *et al.* [22] studied the interconnection of more than two networks with an arbitrary one-to-one correspondence structure. Sanchez-Garcia *et al.* [23] employed eigenvalue interlacing [18] to provide bounds for the Laplacian spectra of an interconnected network with a general interconnection pattern. In addition, in a similar context of structural transition as [1], D'Agostino [24] showed that adding interconnection links among networks causes structural transition. For a class of random network models, specified by an intralayer [25] and an interlayer degree distribution, Radicchi [26] showed when

the correlation between intralayer and interlayer degrees is below a threshold value, the interconnected networks become indistinguishable.

We study the interconnected network $\boldsymbol{G}$ of Radicchi and Arenas [1], and Gomez *et al.* [2], as depicted in Fig. 1. Matrices A and B represent the adjacency matrices of G_A and G_B, respectively. The overall adjacency matrix and Laplacian matrix [18] of the interconnected network $\boldsymbol{G}$ are

$$\boldsymbol{A} = \begin{bmatrix} A & pI \\ pI & B \end{bmatrix} \text{ and } \boldsymbol{L} = \begin{bmatrix} L_A + pI & -pI \\ -pI & L_B + pI \end{bmatrix},$$

where L_A and L_B are the Laplacian matrices of G_A and G_B, respectively, and I is the identity matrix. The eigenvalues of the Laplacian matrix $\boldsymbol{L}$, denoted by $0 = \lambda_1 < \lambda_2 \leq \cdots \leq \lambda_{2N}$, are the solutions of the eigenvalue problem

$$\begin{bmatrix} L_A + pI & -pI \\ -pI & L_B + pI \end{bmatrix} \begin{bmatrix} v_A \\ v_B \end{bmatrix} = \lambda \begin{bmatrix} v_A \\ v_B \end{bmatrix}, \tag{1}$$

where v_A and v_B contain elements of the eigenvector $\boldsymbol{v} = [v_A^T, v_B^T]^T$ corresponding to G_A and G_B, respectively, and satisfy the following eigenvector normalization

$$v_A^T v_A + v_B^T v_B = 2N. \tag{2}$$

The *algebraic connectivity* $\lambda_2(\boldsymbol{L})$ of the interconnected network is the smallest positive eigenvalue of the Laplacian matrix $\boldsymbol{L}$ and the *Fiedler vector* $\boldsymbol{v}_2$ is its corresponding eigenvector. Algebraic connectivity of networks has been studied in depth [18, 20] since Fiedler's seminal paper [19]. Algebraic connectivity quantifies the connectedness of a network and specifies the rate of convergence in a diffusion process [27] to its steady state. The Fiedler vector plays a key role in spectral partitioning of networks (see e.g. [18]).

Superdiffusion occurs if the algebraic connectivity $\lambda_2(\boldsymbol{L})$ of the interconnected network is larger than the algebraic connectivity of each network component [2],

$$\lambda_2(\boldsymbol{L}) > \max\{\lambda_2(L_A), \lambda_2(L_B)\}. \tag{3}$$

Condition (3) indicates that diffusion in the interconnected network $\boldsymbol{G}$ spreads faster than in G_A or G_B if isolated. This condition does not hold for all interconnected networks. Gomez *et al.* [2] proved a necessary condition for superdiffusion is to have $\frac{1}{2}\lambda_2(L_A + L_B) > \max\{\lambda_2(L_A), \lambda_2(L_B)\}$. In this case, the criterion (3) for superdiffusion is met for sufficiently large coupling weights, since the algebraic connectivity $\lambda_2(\boldsymbol{L})$ is a monotone function of the coupling weight p and increases from 0 when $p = 0$, to $\frac{1}{2}\lambda_2(L_A + L_B)$ as $p \to \infty$.

The structural transition phenomenon of [1] can be understood through the behavior of the Fiedler vector of the interconnected network as a function of coupling weight p. For the eigenvalue problem (1), $\lambda = 2p$ and $v_A = -v_B = u \triangleq [1, \ldots, 1]^T$ is always a solution [1, 2]. Therefore, if the coupling weight p is small enough, the algebraic connectivity of the interconnected network is $\lambda_2(\boldsymbol{L}) = \lambda = 2p$. Thus, the Fiedler vector $\boldsymbol{v}_2 = [u^T, -u^T]^T$ corresponding to $\lambda_2(\boldsymbol{L}) = 2p$ indicates that networks G_A and G_B are structurally distinct [1]. By increasing the coupling weight p, the eigenvalue $\lambda = 2p$ may no longer be the smallest positive one. Radicchi and Arenas [1] showed the existence of a structural transition at a threshold value p^* such that for $p > p^*$, the eigenvalue $\lambda = 2p$ exceeds the algebraic connectivity $\lambda_2(\boldsymbol{L})$, thus indicating an abrupt structural transition. Moreover, Radicchi and Arenas [1] argued that the coupling threshold is upper-bounded by one fourth of the algebraic connectivity of the *superpositioned network* G_s with adjacency matrix $A + B$, which is equivalent to

$$p^* \leq \frac{1}{2}\lambda_2\left(\frac{L_A + L_B}{2}\right). \tag{4}$$

Although coupling threshold p^* is a critical quantity for interconnected networks, little is known apart from the upper bound (4). We now explain our new method to find the exact expression for the coupling threshold p^*.

Since elements of the Laplacian matrix $\boldsymbol{L}$ are continuous functions of p, so are its eigenvalues [28]. This implies that the transition in the Fiedler vector of the interconnected network is not a result of any abrupt transition of the eigenvalues of $\boldsymbol{L}$, but rather due to crossing of eigenvalue trajectories as functions of p. Specifically, the Fiedler vector transition occurs precisely at the point where the second and third eigenvalues of $\boldsymbol{L}$ coincide. Therefore, *coupling threshold p^* is such that $\lambda = 2p^*$ is a positive, repeated eigenvalue of $\boldsymbol{L}$.*

As detailed in the Supplemental Material [29, B.i.], we find that repeated eigenvalues occur at $\lambda = 2p^*$ for $N - 1$ different values of p^*, namely $p^* = \frac{1}{2}\lambda_i(Q)$ for $i \in \{2, \cdots, N\}$, where Q can be expressed in the following forms [29, B.ii]:

$$Q \triangleq \bar{L} - \tilde{L}\bar{L}^\dagger\tilde{L} \tag{5}$$

$$= 2(L_A - \frac{1}{2}L_A\bar{L}^\dagger L_A) = 2(L_B - \frac{1}{2}L_B\bar{L}^\dagger L_B) \tag{6}$$

$$= L_A\bar{L}^\dagger L_B = L_B\bar{L}^\dagger L_A, \tag{7}$$

where $\bar{L} \triangleq \frac{1}{2}(L_A + L_B)$, $\tilde{L} \triangleq \frac{1}{2}(L_A - L_B)$, and the superscript † denotes the Moore–Penrose pseudo-inverse [18]. Transition in the algebraic connectivity occurs at the coupling threshold corresponding to the smallest positive eigenvalue of Q, i.e.,

$$p^* = \frac{1}{2}\lambda_2(Q). \tag{8}$$

Furthermore, the coupling threshold p^* can be alternatively obtained as [29, B.iii.]

$$p^* = \frac{1}{\rho(L_A^\dagger + L_B^\dagger)}, \tag{9}$$

where $\rho(\bullet) \triangleq \lambda_N(\bullet)$ denotes the spectral radius [18].

The exact coupling threshold equation (8) depends, in a nonlinear way, on the matrices L_A, L_B, $\bar{L}$, and $\tilde{L}$ in Eq. (5-7), and unveils that the structural transition phenomenon is

jointly caused by A and B. Unfortunately, the exact solution (8) includes the joint influence of the network components *implicitly*.

However, the exact solution for the coupling threshold can lead to several lower and upper bounds for p^* with simple, physically informative expressions. Some of these bounds can be expressed only in terms of of the algebraic connectivity of each isolated network G_A and G_B, as well as the superpositioned network G_s, as [29, B.iv., B.v.]

$$p^* \geq \frac{1}{\lambda_2^{-1}(L_A) + \lambda_2^{-1}(L_B)}, \tag{10}$$

$$p^* \leq \min\{\lambda_2(L_A), \lambda_2(L_B), \frac{1}{2}\lambda_2(\bar{L})\}. \tag{11}$$

We can furthermore find expressions that include *explicit* quantities pertaining to the network components jointly. We refer to such quantities as *interrelation* descriptors. As an example, we have obtained a class of upper bounds $p^* \leq \frac{1}{\tilde{\rho}_{n_A,n_B}}$ which depend on inner product of the eigenvectors of G_A and G_B with tunable accuracy and low computational cost as discussed in details in [29, B.viii.]. For further discussions on the network interrelation concept, readers can refer to [29, C.].

Expression (10) elegantly lower bounds p^* by half of the harmonic mean of $\lambda_2(L_A)$ and $\lambda_2(L_B)$, and *is exact if* $v_{2A} = v_{2B}$. The upper bounds (11) not only include the upper bound (4), proposed in [1], but also exhibit a fundamental property of interconnected networks: *the coupling threshold p^* is upper bounded by the algebraic connectivity of each network component.*

Interestingly, if the algebraic connectivity of one network, say G_A, is much smaller than that of the other network G_B, then the network component with the smallest algebraic connectivity, here G_A, prominently determines the coupling threshold; but neither G_B, nor the superpositioned network G_s, play a major role. Indeed, if $K \triangleq \lambda_2(L_B)/\lambda_2(L_A) > 3$, then [29, B.vi.]

$$\frac{K}{1+K}\lambda_2(L_A) < p^* \leq \lambda_2(L_A). \tag{12}$$

A corollary of (12) is if one of the network components has a vanishing algebraic connectivity, which is the case for a class of scale-free networks where $\lambda_2 \sim (\ln N)^{-2}$ [30], then $p^* \to 0$, indicating the transition point also disappears. Therefore, in such cases, even a very small coupling weight p leads to structural transition. This result is physically intuitive because a network with a small algebraic connectivity is vulnerable and loses its unity in response to external perturbations such as removal of a few edges/nodes or, as our analysis suggests, a weak coupling to another network.

Considering the opposite situation where the algebraic connectivity values of both networks are close to each other, we can show $p^* > \frac{1}{2}\max\{\lambda_2(L_A), \lambda_2(L_B)\}$ if the Fielder vectors are far from being parallel (see [29, B.vii.]). As a consequence, for each coupling weight p satisfying $\frac{1}{2}\max\{\lambda_2(L_A), \lambda_2(L_B)\} < p \leq p^*$, we have

$$\lambda_2(\boldsymbol{L}) = 2p > \max\{\lambda_2(L_A), \lambda_2(L_B)\}. \tag{13}$$

Comparison of (13) with the superdiffusion criterion (3) reveals the counterintuitive finding that *superdiffusion, a synergistic characteristic phenomenon of an interconnected network, can occur for values of $p < p^*$, where the network components function distinctly!*

As mentioned above, the condition that Fielder vectors of G_A and G_B are far from being parallel is necessary for superdiffusion before structural transition. We find that this condition is indeed general to superdiffusion, regardless of structural transition; because close-to-parallel Fielder vectors of G_A and G_B yields $\lambda_2(\frac{L_A+L_B}{2}) \simeq \frac{\lambda_2(L_A)+\lambda_2(L_B)}{2}$, thus the necessary condition for superdiffusion, i.e., $\lambda_2(\frac{L_A+L_B}{2}) > \max\{\lambda_2(L_A), \lambda_2(L_B)\}$ can never be satisfied even for $p \to \infty$. This condition has a very interesting physical interpretation. When $p \to \infty$, corresponding nodes in G_A and G_B become a single entity. According to the important role of the Fiedler vector in graph partitioning, having close-to-orthogonal Fiedler vectors of G_A and G_B means that links of G_B connect those nodes that are far from each other in G_A, and vice versa. Therefore, with close-to-orthogonal Fiedler vectors of G_A and G_B, the overall interconnected network gains increased connectivity among its nodes compared to each isolated component, thus making superdiffusion feasible.

It is important to distinguish between speed of diffusion, determined by the smallest positive eigenvalues of the Laplacian matrix, and the mode of diffusion, determined by the corresponding eigenvectors. Superdiffusion concerns the speed of diffusion, while structural transition corresponds to an abrupt change in modes of diffusion. It would be a wrong idea to assume $p < p^*$ indicate that G_A and G_B are independents (expect for the trivial case of $p = 0$). The key point is that having $p < p^*$ simply implies that G_A and G_B are distinguishable. Before the structural transition the network components do interact with each other, and as we showed, can even positively favor the diffusion process speed as the result of increased overall connectivity in the interconnected network.

To illustrate our analytical assertions, we perform several numerical simulations. We generate an interconnected network with $N = 1000$, where the graph G_A is a scale-free network according to the configuration model [31] with exponent $\gamma = 3$, and G_B is a random geometric network [32] with threshold distance $r_c = \sqrt{\frac{5\log N}{\pi N}}$. For generating the random geometric network, N nodes are uniformly and independently distributed in $[0,1]^2$ at random, and nodes of at most distance r_c are connected to each other. For these networks, $\lambda_2(L_A) \simeq 0.355$ and $\lambda_2(L_B) \simeq 0.332$. Fig. 2 shows the algebraic connectivity $\lambda_2(L)$ of the interconnected network as a function of the coupling weight p, and

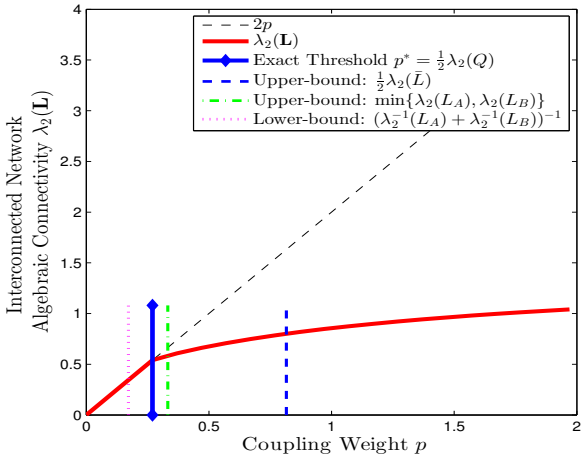

FIG. 2. Algebraic connectivity $\lambda_2(\boldsymbol{L})$ of an interconnected network with scale-free G_A and random geometric G_B as a function of the coupling weight p. For $p < p^* \simeq 0.27$, algebraic connectivity is $\lambda_2(\boldsymbol{L}) = 2p$. For $p > p^*$, eigenvalue $\lambda = 2p$ is no longer the algebraic connectivity of the interconnected network; thus, denoting a structural transition at $p = p^*$.

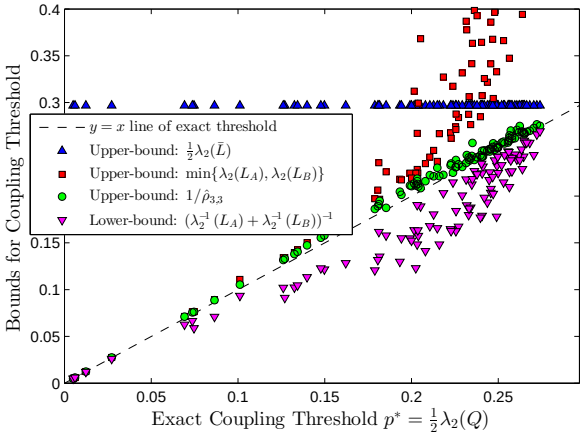

FIG. 3. Bounds for the coupling threshold versus the exact values for a set of interconnected networks with identical averaged network. For each generated network, we compute different bounds for the coupling threshold and compare them with the exact value. The closer to the black dashed line $y = x$, the more accurate the bounds.

illustrates that Eq. (8) predicts the coupling threshold exactly. Furthermore, this simulation supports the analytic results for bounds in (11) and (10).

In order to investigate structural implications of interconnected networks, we design numerical experiments emphasizing the role of network interrelation. We generate a set of interconnected networks with identical superpositioned networks. Therefore, differences in the outcomes do not depend on the superpositioned network. We generate $A = [a_{ij}]$ and $B = [b_{ij}]$ according to the following rule: $a_{ij} = a_{ji} = p_{ij}w_{ij}$ and $b_{ij} = b_{ji} = (1 - p_{ij})w_{ij}$, where w_{ij} is an element of the weighted Karate Club adjacency matrix [33, Fig. 3], and p_{ij} is identically independently distributed on $[0, 1]$ for $j < i$. Fig. 3 shows different bounds for the coupling threshold versus the exact values. The upper bound $\frac{1}{2}\lambda_2(\bar{L})$ remains constant, even though the exact threshold p^* has a broad distribution. When p^* is small, the upper bound $\frac{1}{2}\lambda_2(\bar{L})$ is loose, while the upper bound $\min\{\lambda_2(A),\lambda_2(B)\}$ is tight, as supported by Eq. (12). If one network component possesses a relatively small algebraic connectivity, Eq. (12) predicts that the coupling threshold p^* is determined by the algebraic connectivity of that component.

In conclusion, we derive the exact critical value p^* for the coupling weight in an interconnected network of Fig. 1. In addition to graph properties of each network components individually, we find that the inner product of Fielder vectors of network components is an important interrelation descriptor for the structural transition phenomenon (see [29, A.iv. Fig. 4] for supporting numerical experiments). Other interrelation descriptors, such as the commonly used degree correlation [34–37], do not necessarily yield similar results [29, A.iv. Fig.5]. Even though the analysis has been performed for interconnection of two networks, we demonstrate in [29, D.] that our method can be readily generalized to multiple, interconnected networks.

Our exact solution reveals diversified behaviors in interconnected networks; encompassing the case where the slightest coupling between network components results in a structural transition, as well as the case where coupling strength that is sufficiently large to cause superdiffusion is not large enough to cause structural transition. This emphasizes the importance and power of deliberate design for interconnected networks. In particular, our finding of superdiffusion without structural transition encourages further exploration of dynamical processes and interconnection architectures which allow the very benefits of interconnections while preserving the autonomy of each subsystem.

Acknowledgement. This work has been supported by the National Science Foundation Award CIF-1423411. Authors would like to thank Filippo Radicchi, Alex Arenas, Aram Vajdi, Joshua Melander, and anonymous reviewers for their helpful suggestions to improve this manuscript.

[1] F. Radicchi and A. Arenas, Nat. Phys. **9**, 717 (2013).
[2] S. Gómez, A. Diaz-Guilera, J. Gómez-Gardeñes, C. J. Pérez-Vicente, Y. Moreno, and A. Arenas, Phys. Rev. Lett. **110**, 028701 (2013).
[3] Note1, such extensions have been present in classical sociology literature such as H. C. White, S. A. Boorman, and R. L. Breiger, Am. J. Sociol. pp. 730–780 (1976), which even dates back to L. von Wiese, *Sociology* (Oskar Piest, New York, 1941).
[4] M. Kivelä, A. Arenas, M. Barthelemy, J. P. Gleeson,

Y. Moreno, and M. A. Porter, J. Comp. Netw. **2**, 203 (2013).
[5] S. Boccaletti, G. Bianconi, R. Criado, C. Del Genio, J. Gómez-Gardeñes, M. Romance, I. Sendiña-Nadal, Z. Wang, and M. Zanin, Phys. Rep. **544**, 1 (2014).
[6] J. Gao, S. V. Buldyrev, S. Havlin, and H. E. Stanley, Phys. Rev. Lett. **107**, 195701 (2011).
[7] J. Gao, S. Buldyrev, S. Havlin, and H. Stanley, Phys. Rev. E **85**, 066134 (2012).
[8] E. Estrada and J. Gómez-Gardeñes, Phys. Rev. E **89**, 042819 (2014).
[9] M. De Domenico, A. Solé-Ribalta, S. Gómez, and A. Arenas, Proc. Natl. Acad. Sci. p. 201318469 (2014).
[10] S. V. Buldyrev, R. Parshani, G. Paul, H. E. Stanley, and S. Havlin, Nature **464**, 1025 (2010).
[11] Y. Hu, B. Ksherim, R. Cohen, and S. Havlin, Phys. Rev. E **84**, 066116 (2011).
[12] A. Saumell-Mendiola, M. Á. Serrano, and M. Boguñá, Phys. Rev. E **86**, 026106 (2012).
[13] M. Dickison, S. Havlin, and H. E. Stanley, Phys. Rev. E **85**, 066109 (2012).
[14] H. Wang, Q. Li, G. DAgostino, S. Havlin, H. E. Stanley, and P. Van Mieghem, Phys. Rev. E **88**, 022801 (2013).
[15] F. Sahneh, C. Scoglio, and F. Chowdhury, in *P. Amer. Contr. Conf.* (2013), pp. 2307–2312, ISSN 0743-1619.
[16] J. Aguirre, R. Sevilla-Escoboza, R. Gutiérrez, D. Papo, and J. Buldu, Phys. Rev. Lett. **112**, 248701 (2014).
[17] Note2, such a topology is sometimes called a multiplex or more generally a multilayer network [4].
[18] P. Van Mieghem, *Graph Spectra for Complex Networks* (Cambridge Univ Pr, 2011).
[19] M. Fiedler, Czechoslovak Mathematical Journal **23**, 298 (1973).
[20] N. M. M. de Abreu, Linear algebra and its applications **423**, 53 (2007).
[21] J. Martín-Hernández, H. Wang, P. Van Mieghem, and G. D'Agostino, Physica A **404**, 92 (2014).
[22] A. Solé-Ribalta, M. De Domenico, N. E. Kouvaris, A. Díaz-Guilera, S. Gómez, and A. Arenas, Phys. Rev. E **88**, 032807 (2013).
[23] R. J. Sánchez-García, E. Cozzo, and Y. Moreno, Phys. Rev. E **89**, 052815 (2014).
[24] G. D'Agostino, in *Nonlinear Phenomena in Complex Systems: From Nano to Macro Scale* (Springer, 2014), pp. 111–131.
[25] Note3, intralayer links denote those within a single network, while interlayer links are those that connect two different networks.
[26] F. Radicchi, Phys. Rev. X **4**, 021014 (2014).
[27] Note4, the dynamic equation for a diffusion process on a graph with Laplacian matrix L follows $\dot{x} = -Lx$, which is the discretized equivalent of the heat equation $\partial_t \phi = \nabla^2 \phi$ for a continuous medium. Eq. $\dot{x} = -Lx$ can also describe first-order consensus dynamics [see, e.g., R. Olfati-Saber, J. A. Fax, and R. M. Murray, Proc. IEEE **95**, 215 (2007)], analogous to a linearized synchronization equation [see, e.g., A. Arenas, A. Díaz-Guilera, J. Kurths, Y. Moreno, and C. Zhou, Phys. Rep. **469**, 93 (2008)].
[28] M. Zedek, Proc. Amer. Math. Soc., Proc. **16**, 78 (1965).
[29] See Supplemental Material at [URL] for mathematical proofs, additional numerical simulations, and extensions to more than two interconnected networks.
[30] A. Samukhin, S. Dorogovtsev, and J. Mendes, Phys. Rev. E **77**, 036115 (2008).
[31] B. Bollobás, European Journal of Combinatorics **1**, 311 (1980).
[32] M. Penrose, *Random geometric graphs*, vol. 5 (Oxford University Press Oxford, 2003).
[33] W. W. Zachary, J. Anthropol. Res. pp. 452–473 (1977).
[34] J. Y. Kim and K.-I. Goh, Phys. Rev. Lett. **111**, 058702 (2013).
[35] B. Min, S. Do Yi, K.-M. Lee, and K.-I. Goh, Phys. Rev. E **89**, 042811 (2014).
[36] V. Nicosia and V. Latora, arXiv preprint arXiv:1403.1546 (2014).
[37] V. Gemmetto and D. Garlaschelli, Sci. Rep. **5** (2015).

Supplemental Material for "Exact Coupling Threshold for Structural Transition Reveals Diversified Behaviors in Interconnected Networks"

Faryad Darabi Sahneh,[1,*] Caterina Scoglio,[1] and Piet Van Mieghem[2]

[1]*Electrical and Computer Engineering Department, Kansas State University*
[2]*Faculty of Electrical Engineering, Mathematics, and Computer Science, Delft University of Technology, Delft, The Netherlands*

Contents

This Supplemental Material contains extra simulation results, as well as details of the proofs and analytical deductions quoted in the main text of the Letter.

A. ADDITIONAL NUMERICAL SIMULATIONS

A.i. An Illustrative Example for Structural Transition

When the coupling weight is less than the threshold value, i.e., $p < p^*$, the Fiedler vector of the interconnected network $\boldsymbol{G}$ is $v_2(\boldsymbol{L}) = \begin{bmatrix} u \\ -u \end{bmatrix}$, indicating that nodes of G_A are distinguishable from nodes of G_B. When $p > p^*$, the interconnected network $\boldsymbol{G}$ functions as a whole and nodes of G_A are no longer distinguishable from nodes of G_B. To illustrate this, Fig. 2 shows the response of diffusion dynamics $\dot{\boldsymbol{X}} = -\boldsymbol{L}\boldsymbol{X}$, for two cases where coupling is weak and strong. Here $\boldsymbol{X} \triangleq [X_{A,1}, \ldots, X_{A,N}, X_{B,1}, \ldots, X_{B,N}]^T$ denotes the nodal states of the interconnected network $\boldsymbol{G}$, and X_A and X_B are those related to nodes of graphs G_A and G_B, respectively.

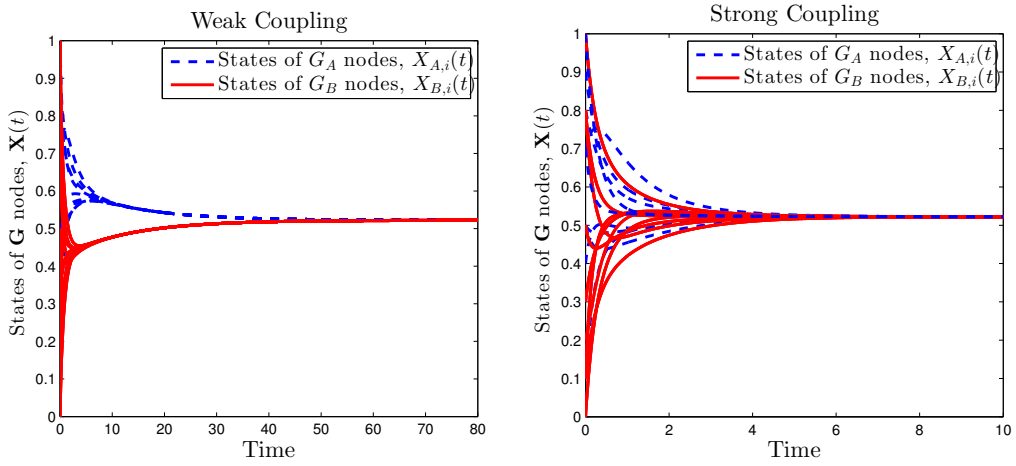

FIG. 1: Diffusion process $\dot{\boldsymbol{X}} = -\boldsymbol{L}\boldsymbol{X}$ for the interconnected network of Fig. 1 in the main text. When coupling is weak (left), i.e., the coupling weight is below the coupling threshold, the two networks function separately: nodal states of G_A (dashed blue) and G_B (solid red) converge together separately, and later, the whole interconnected network slowly converges to a single steady-state value. When coupling is strong (right), i.e., the coupling weight is larger than the coupling threshold, it is not possible to distinguish nodes of the two networks: the interconnected network functions as a whole.

A.ii. An Illustrative Example for Superdiffusion and Structural Transition

The purpose of this illustrative example is to show the behavior of diffusion dynamics when superdiffusion happens while network components function distinctly. Fig. 2 shows the response of the diffusion dynamics $\dot{\boldsymbol{X}} = -\boldsymbol{L}\boldsymbol{X}$ for different values of the coupling weight p.

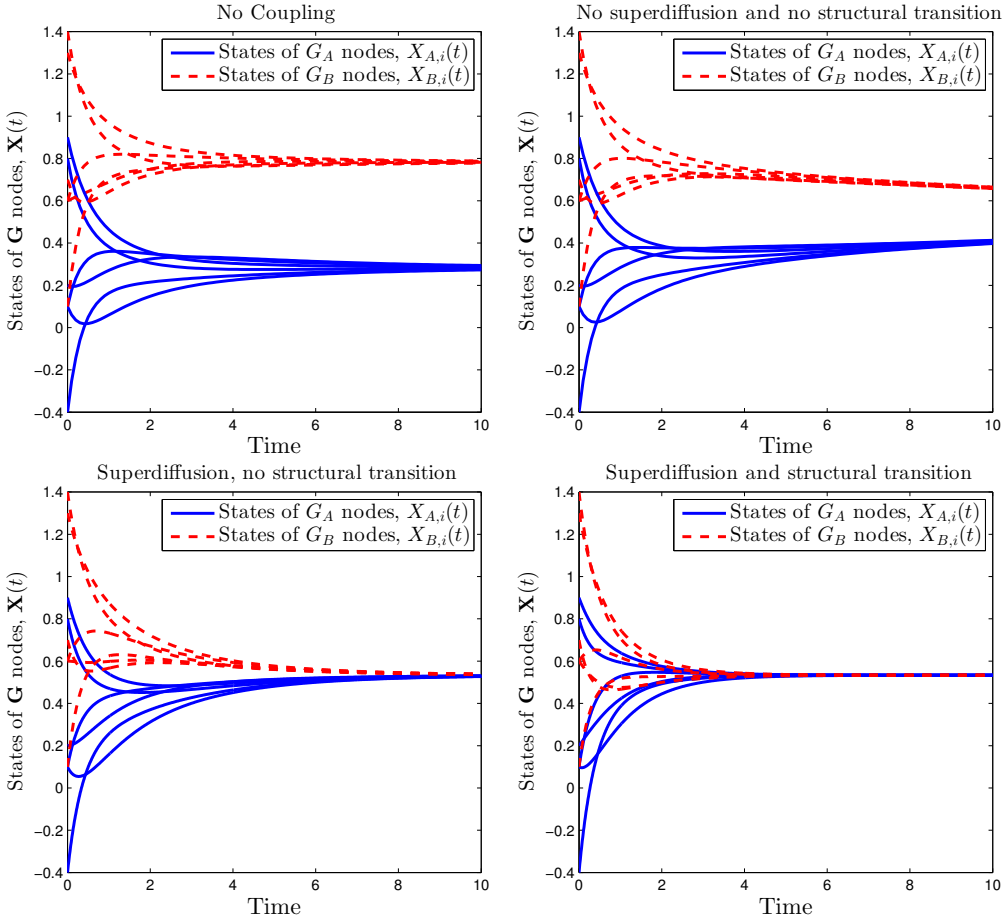

FIG. 2: Diffusion process$\dot{\boldsymbol{X}} = -\boldsymbol{L}\boldsymbol{X}$ for different values of coupling weight p. **Top left**: There is no coupling ($p = 0$): each network component reach its own steady state. **Top right:** The coupling weight is much less than the coupling threshold. Here nodal states of G_A (solid blue) and G_B (dashed red) converge together separately, and later, the whole interconnected network slowly converges to a same steady state. **Bottom left:** The coupling weight is still below the coupling threshold, however it is large enough that superdiffusion can take place, i.e., $\frac{1}{2}\max\{\lambda_2(L_A) < p < p^*$. Here still the two components function distinctly, yet the overall diffusion of the interconnected network happens faster than diffusion processes in case of no coupling, shown in top left figure. **Bottom right:** The coupling weight is larger than the threshold, i.e., $p > p^*$. It is not possible to distinguish nodes of the two networks and the interconnected network functions as a whole.

A.iii. Example Simulations for Nonvanishing Coupling Threshold

As predicted by our model, the threshold goes to zero when one of the network components has vanishing algebraic connectivity. We have performed simulations for the case where both network components are Erdös Rényi, which are expanders in the connected region. Specifically, we have performed the simulation for two sizes $N = 2000$ and $N = 500$. And for each one, Fig. 3 reported two sample outputs. Even though this simulation is not exhaustive in any sense, it hints us that the size of the network does not play a major role here. Rather, it is the algebraic connectivity of the components and their interrelation that are major players, as predicted by our analytical results.

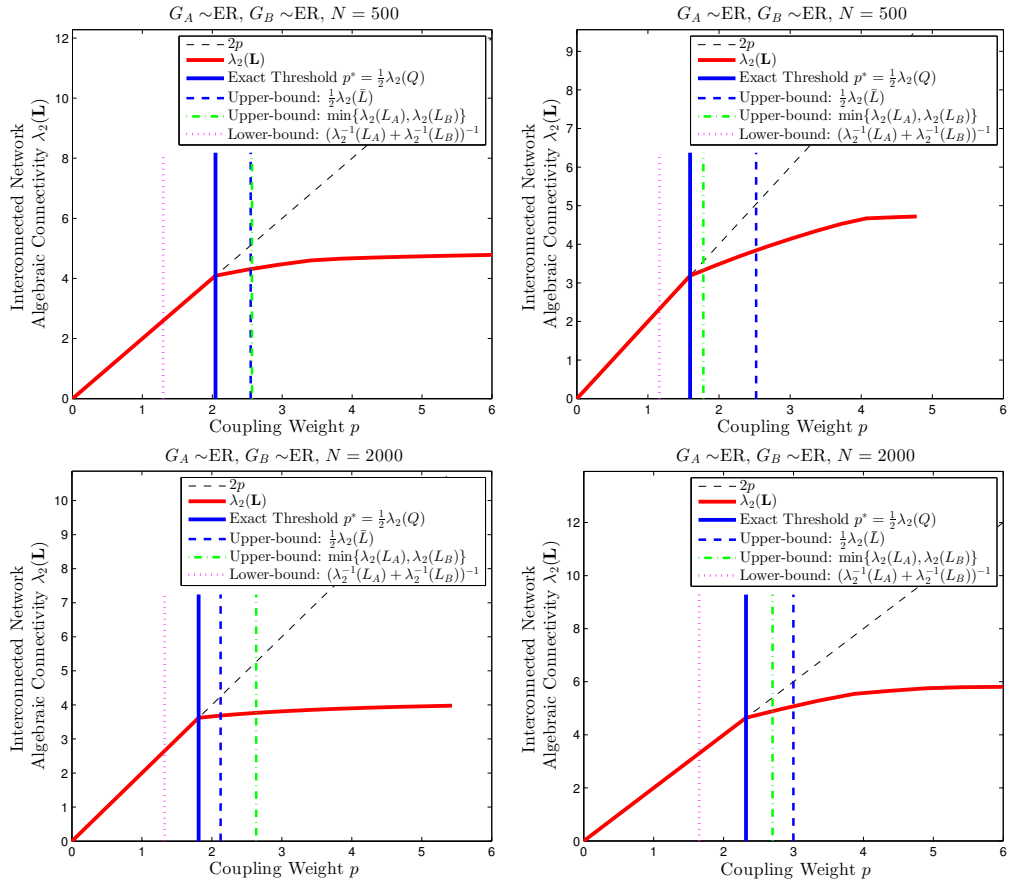

FIG. 3: Algebraic connectivity $\lambda_2(\boldsymbol{L})$ of different interconnected networks as a function of coupling weight p. Here, G_A and G_B are Erdös Rényi graphs with parameters $p_A = 2\frac{log(N)}{N}$ and $p_B = 1.8\frac{log(N)}{N}$, respectively. Top panel shows two realization of such interconnected network with $N = 500$, while the bottom panel shows two realization for $N = 2000$. As can be seen, different realizations can lead to different accuracy of upper bounds $\frac{1}{2}\lambda_2(\bar{L})$ and $\min\{\lambda_2(L_A), \lambda_2(L_B)\}$.

A.iv. Fielder Vectors Inner Product as an Interrelation Measure

We generate a set of interconnected networks with fixed adjacency matrix A, and construct the adjacency matrix of G_B as $B = P^{-1}AP$, where P is a randomly chosen permutation matrix, so that G_B is the same graph as G_A; however, with different node labels. Hence, G_A and G_B are isomorphic and have identical graph properties. As a consequence, different outcomes are due to the interrelation between G_A and G_B. In our simulations, A is the adjacency matrix of the weighted Karate Club network — adopted from Zackary [1, Fig. 3] — with $N = 34$ nodes. We uniformly and independently select m nodes at random and shuffle their labels, and then construct the corresponding permutation matrix P. We repeat this procedure 10 times for each $m = 2, ..., N$, resulting in a total of $10 \times (34 - 1) = 330$ interconnected networks. For each such generated interconnected network, Fig. 4 shows several bounds for the coupling threshold plotted versus the exact value. The upper bound $\min\{\lambda_2(A),\lambda_2(B)\}$ and lower bound $(\lambda_2^{-1}(A) + \lambda_2^{-1}(B))^{-1}$ are always constant, because these values only depend on the graph properties of G_A and G_B, which are kept identical.

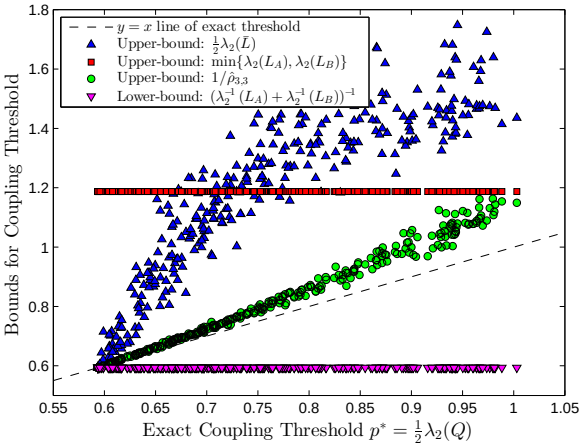

FIG. 4: Bounds for the coupling threshold versus the exact values for a set of interconnected networks where network G_A and G_B are isomorphic, and thus have identical graph properties. For each generated network, we compute different bounds for the coupling threshold and compare them with the exact value. The closer to the black dashed line, the more accurate the bounds.

Fig. 5 shows the exact value p^* of the coupling threshold versus the inner product $v_2^T(L_A)v_2(L_B)$ of the Fiedler vectors of L_A and L_B. We observe a significant negative correlation between the coupling threshold and the inner product $v_2^T(L_A)v_2(L_B)$. The coupling threshold p^* is maximal when the two networks are uncorrelated (i.e., $|v_2^T(L_A)v_2(L_B)| \to 0$ implying that the Fiedler vectors $v_2(L_A)$ and $v_2(L_B)$ tend to be orthogonal) and p^* decreases when the two networks become more correlated ($|v_2^T(L_A)v_2(L_B)| \to 1$). Therefore a significant negative correlation between the coupling threshold p^* and the absolute value of the inner product $|v_2^T(L_A)v_2(L_B)|$ of the Fiedler vectors of G_A and G_B is observed: the coupling threshold p^* is maximal, when the two networks are uncorrelated (i.e., $|v_2^T(L_A)v_2(L_B)| \to 0$) and p^* decreases when the two networks are more correlated ($|v_2^T(L_A)v_2(L_B)| \to 1$).

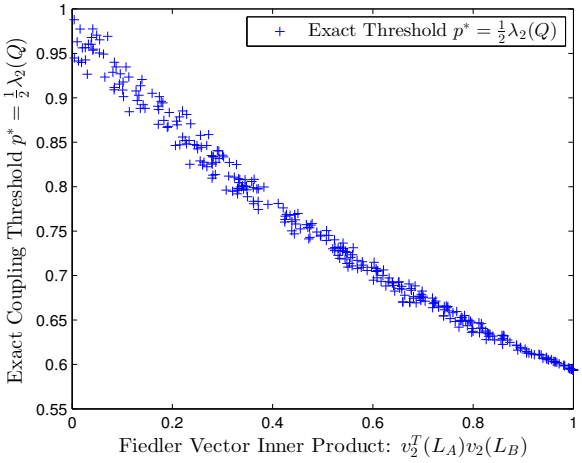

FIG. 5: Exact coupling threshold versus Fiedler vectors inner product when G_B is a relabeling of G_A.

As remarked in the main text, the correlation between G_A and G_B, measured in terms of their Fiedler vectors inner product differs generaly from other correlation metrics such as degree correlation. Indeed, Figure 6 plots the exact value p^* of the coupling threshold versus the correlation coefficient $r(d_A, d_B)$ between degree vectors of G_A and G_B and illustrates a much weaker correlation between the coupling threshold p^* and the degree correlation coefficient $r(d_A, d_B)$.

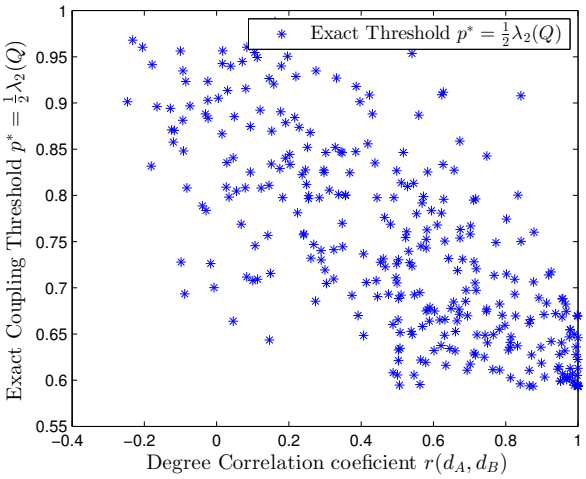

FIG. 6: Exact coupling threshold versus the correlation coefficent $r(d_A, d_B)$ between degree vectors of G_A and G_B.

B. PROOFS AND ANALYTIC DEDUCTIONS

B.i. Derivations for the Exact Coupling Threshold p^* Expressed in (8)

Our approach to finding the exact value of coupling threshold p^* employs an eigenvalue sensitivity analysis. The key idea is that while a first-order differentiation of eigenvalue equation (1) determines the eigenvalue/eigenvector derivatives for distinct eigenvalues [2], this method is not applicable to repeated eigenvalues [3]. Hence, in order to determine when $\lambda = 2p$ is a repeated eigenvalue, we study the system of equations for the eigenvalue and eigenvector derivatives with respect to p and look for a critical value of p^* such that a unique solution does not exist at $\lambda = 2p$.

Differentiating (1) and (2) with respect to p yields the governing equations for the eigenderivatives $\frac{dv_A}{dp}$, $\frac{dv_B}{dp}$, and $\frac{d\lambda}{dp}$

$$\begin{bmatrix} L_A + pI - \lambda I & -pI & -V_A \\ -pI & L_B + pI - \lambda I & -V_B \\ -V_A^T & -V_B^T & 0 \end{bmatrix} \begin{bmatrix} \frac{dv_A}{dp} \\ \frac{dv_B}{dp} \\ \frac{d\lambda}{dp} \end{bmatrix} = \begin{bmatrix} V_B - V_A \\ V_A - V_B \\ 0 \end{bmatrix}. \tag{B.1}$$

At $\lambda = 2p$, $V_A = -V_B = u$, we get

$$\begin{bmatrix} L_A - pI & -pI & -u \\ -pI & L_B - pI & u \\ -u^T & u^T & 0 \end{bmatrix} \begin{bmatrix} \frac{dv_A}{dp} \\ \frac{dv_B}{dp} \\ \frac{d\lambda}{dp} \end{bmatrix} = \begin{bmatrix} -2u \\ 2u \\ 0 \end{bmatrix}. \tag{B.2}$$

As expected, for $\lambda = 2p$ and $v_A = -v_B = u$, $\frac{dv_A}{dp} = \frac{dv_B}{dp} = \mathbf{0}$ and $\frac{d\lambda}{dp} = 2$ always satisfies (B.2). However, the key idea is that when $\lambda = 2p$ is a repeated eigenvalue, the eigenderivative equation (B.2) does not have a unique solution. This occurs when the matrix

$$W \triangleq \begin{bmatrix} L_A - pI & -pI & -u \\ -pI & L_B - pI & u \\ -u^T & u^T & 0 \end{bmatrix} \tag{B.3}$$

is singular. A singular matrix possesses a zero eigenvalue. Hence, the coupling threshold p^* must obey $W(p^*)\boldsymbol{x} = 0$, explicitly, p^* is the solution of the generalized eigenvalue problem:

$$\begin{bmatrix} L_A & \mathbf{0} & -u \\ \mathbf{0} & L_B & u \\ -u^T & u^T & 0 \end{bmatrix} \boldsymbol{x} = p^* \begin{bmatrix} I & I & \mathbf{0} \\ I & I & \mathbf{0} \\ \mathbf{0} & \mathbf{0} & 0 \end{bmatrix} \boldsymbol{x}. \tag{B.4}$$

Applying the coordinate change $\boldsymbol{y} = T\boldsymbol{x}$, where the orthonormal transformation T is defined as

$$T = \begin{bmatrix} \frac{1}{\sqrt{2}} I & \frac{1}{\sqrt{2}} I & \mathbf{0} \\ -\frac{1}{\sqrt{2}} I & \frac{1}{\sqrt{2}} I & \mathbf{0} \\ \mathbf{0} & \mathbf{0} & 1 \end{bmatrix}, \tag{B.5}$$

to the generalized eigenvalue problem (B.4), we obtain

$$\begin{bmatrix} \frac{L_A + L_B}{2} & \frac{L_A - L_B}{2} & -\sqrt{2}u \\ \frac{L_A - L_B}{2} & \frac{L_A + L_B}{2} & \mathbf{0} \\ -\sqrt{2}u^T & \mathbf{0} & 0 \end{bmatrix} \boldsymbol{y} = p^* \begin{bmatrix} 2I & \mathbf{0} & \mathbf{0} \\ \mathbf{0} & \mathbf{0} & \mathbf{0} \\ \mathbf{0} & \mathbf{0} & 0 \end{bmatrix} \boldsymbol{y}. \tag{B.6}$$

Multiplying the first row of both sides by u^T yields $\boldsymbol{y} = [y_1^T \ y_2^T \ 0]^T$. Therefore, the generalized eigenvalue problem (B.4) reduces to

$$\bar{L} y_1 + \tilde{L} y_2 = 2p^* y_1, \tag{B.7}$$

$$\tilde{L} y_1 + \bar{L} y_2 = 0, \tag{B.8}$$

where $\bar{L}$ and $\tilde{L}$ are defined as

$$\bar{L} \triangleq \frac{L_A + L_B}{2} \text{ and } \tilde{L} \triangleq \frac{L_A - L_B}{2}. \tag{B.9}$$

The matrix $\bar{L}$ is singular and thus cannot be inverted. Using the notion of Moore Penrose pseudo-inverse $\bar{L}^\dagger$, defined [4] as

$$\bar{L}^\dagger \triangleq \sum_{i=2}^{N} \frac{1}{\lambda_i(\bar{L})} v_i(\bar{L}) v_i^T(\bar{L}) = (\bar{L} + \frac{1}{N} uu^T)^{-1} - \frac{1}{N} uu^T, \tag{B.10}$$

where v_i's are the normalized eigenvectors of $\bar{L}$, i.e., $\bar{L}v_i = \lambda_i(\bar{L})v_i$ and $v_i^T v_i = 1$, we have $\tilde{L}\bar{L}^\dagger\bar{L} = \tilde{L}$. Hence, multiplying both sides of (B.8) by $\tilde{L}\bar{L}^\dagger$ from left, we find that $\tilde{L}y_2 = -\tilde{L}\bar{L}^\dagger\tilde{L}y_1$. Replacing $\tilde{L}y_2$ by $-\tilde{L}\bar{L}^\dagger\tilde{L}y_1$ in (B.7) yields the eigenvalue equation

$$Qy_1 = 2p^* y_1, \tag{B.11}$$

where the $N \times N$ matrix Q is defined as $Q \triangleq \bar{L} - \tilde{L}\bar{L}^\dagger\tilde{L}$. Therefore, repeated eigenvalues occur at $\lambda = 2p^*$ for the values of $p^* = \frac{1}{2}\lambda_i(Q)$, for $i \in \{1, \cdots, N\}$. For the transition in algebraic connectivity, the coupling threshold is the smallest positive solution $p^* = \frac{1}{2}\lambda_2(Q)$. In section E.ii, we propose an alternative approach to determine p^* through directly finding zeros of $\det(W)$.

B.ii. Re-expressing Q as (6) and (7)

In order to show (6), we use the definitions of $\bar{L}$ and $\tilde{L}$ in (B.9) and properties of Moore Penrose pseudo-inverse operator [4] to obtain:

$$\begin{aligned}
Q &= \bar{L} - \tilde{L}\bar{L}^\dagger\tilde{L} \\
&= \bar{L} - (\bar{L} - L_B)\bar{L}^\dagger(\bar{L} - L_B) \\
&= \bar{L} - \bar{L}\bar{L}^\dagger\bar{L} + L_B\bar{L}^\dagger\bar{L} - L_B\bar{L}^\dagger L_B + \bar{L}\bar{L}^\dagger L_B \\
&= \bar{L} - \bar{L} + L_B - L_B\bar{L}^\dagger L_B + L_B \\
&= 2\left(L_B - \frac{1}{2}L_B\bar{L}^\dagger L_B\right).
\end{aligned} \tag{B.12}$$

Similarly, it can be shown that $Q = 2\left(L_A - \frac{1}{2}L_A\bar{L}^\dagger L_A\right)$. Relation (7) follows as

$$\begin{aligned}
Q &= \bar{L} - \tilde{L}\bar{L}^\dagger\tilde{L} \\
&= \bar{L} - (L_A - \bar{L})\bar{L}^\dagger(\bar{L} - L_B) \\
&= \bar{L} - L_A\bar{L}^\dagger\bar{L} + L_A\bar{L}^\dagger L_B + \bar{L}\bar{L}^\dagger\bar{L} - \bar{L}\bar{L}^\dagger L_B \\
&= \bar{L} - L_A + L_A\bar{L}^\dagger L_B + \bar{L} - L_B \\
&= \left[2\bar{L} - (L_A + L_B)\right] + L_A\bar{L}^\dagger L_B \\
&= L_A\bar{L}^\dagger L_B,
\end{aligned} \tag{B.13}$$

and similarly, $Q = L_B\bar{L}^\dagger L_A$.

B.iii. Derivations of Expression (9) for p^*

According to (7), $2p^*$ is a positive eigenvalue of $Q = L_B\bar{L}^\dagger L_A = L_B(\frac{L_A+L_B}{2})^\dagger L_A = 2L_B(L_A+L_B)^\dagger L_A$. Therefore, $\frac{1}{p^*}$ is a positive eigenvalue of $\left[L_B(L_A+L_B)^\dagger L_A\right]^\dagger = L_A^\dagger(L_A+L_B)L_B^\dagger = (L_A^\dagger + L_B^\dagger)$. Furthermore, since $2p^*$ is the smallest positive eigenvalue of Q, then $\frac{1}{p^*}$ must be the largest eigenvalue of $(L_A^\dagger + L_B^\dagger)$, which demonstrates (9).

B.iv. Derivations of the Lower Bound (10)

According to (9),

$$p^* = \frac{1}{\rho(L_A^\dagger + L_B^\dagger)} \geq \frac{1}{\rho(L_A^\dagger) + \rho(L_B^\dagger)} = \frac{1}{\lambda_2^{-1}(L_A) + \lambda_2^{-1}(L_B)}, \tag{B.14}$$

where we have used the inequality $\rho(L_A^\dagger + L_B^\dagger) \leq \rho(L_A^\dagger) + \rho(L_B^\dagger)$ and the fact that $\rho(L_A^\dagger) = \lambda_2^{-1}(L_A)$ and $\rho(L_B^\dagger) = \lambda_2^{-1}(L_B)$. Therefore, the coupling threshold p^* is lower-bounded by $\left(\lambda_2^{-1}(L_A) + \lambda_2^{-1}(L_B)\right)^{-1}$, yielding (10). The above inequality is strict when $v_2(L_A) \neq v_2(L_B)$ because $\rho(L_A^\dagger + L_B^\dagger) = \rho(L_A^\dagger) + \rho(L_B^\dagger)$ only when $v_2(L_A) = v_2(L_B)$.

B.v. Derivations of the Upper Bound (11)

In order to show (11), we can use expression (6) for $Q = 2\left(L_B - \frac{1}{2}L_B\bar{L}^\dagger L_B\right)$. Since both $L_B\bar{L}^\dagger L_B$ and $L_A\bar{L}^\dagger L_A$ are positive semi-definite, $p^* = \frac{1}{2}\lambda_2(Q) \leq \frac{1}{2}\lambda_2(2L_B) = \lambda_2(L_B)$. Similarly, $p^* \leq \lambda_2(L_A)$. Therefore, combining these upper bounds with 4, we get $p^* \leq \min\{\lambda_2(L_A), \lambda_2(L_B), \frac{1}{2}\lambda_2(\bar{L})\}$.

B.vi. Bound (12) in the Case $\lambda_2(L_A) < \frac{1}{3}\lambda_2(L_B)$

Suppose $K = \lambda_2(L_B)/\lambda_2(L_A) > 3$. When $\lambda_2(L_A) < \frac{1}{3}\lambda_2(L_B)$, we reported in the main text that $\min\{\lambda_2(L_A), \lambda_2(L_B), \frac{1}{2}\lambda_2(\bar{L})\} = \lambda_2(L_A)$. In order to prove this, we have used the inequality [5]

$$\lambda_2(\bar{L}) \geq \frac{\lambda_2(L_A) + \lambda_2(L_B)}{2}, \tag{B.15}$$

combined with the inequality $\lambda_2(L_B) > 3\lambda_2(L_A)$ to obtain

$$\frac{1}{2}\lambda_2(\bar{L}) \geq \frac{1}{2}\frac{\lambda_2(L_A) + \lambda_2(L_B)}{2} > \frac{1}{2}\frac{\lambda_2(L_A) + 3\lambda_2(L_A)}{2} = \lambda_2(L_A), \tag{B.16}$$

thus proving the claim $\min\{\lambda_2(L_A), \lambda_2(L_B), \frac{1}{2}\lambda_2(\bar{L})\} = \lambda_2(L_A)$.

From the lower bound (10),

$$p^* \geq \frac{1}{\lambda_2^{-1}(L_A) + \lambda_2^{-1}(L_B)} = \frac{1}{1 + \frac{\lambda_2(L_A)}{\lambda_2(L_B)}}\lambda_2(L_A) \geq \frac{1}{1 + \frac{1}{K}}\lambda_2(L_A) = \frac{K}{K+1}\lambda_2(L_A).$$

Therefore, bound (12) is obtained.

B.vii. Superdiffusion condition (13) when $\lambda_2(L_A) \simeq \lambda_2(L_B)$

We investigate whether it is possible that an interconnected network achieves superdiffusion without going through structural transition. As discussed in the main text, this situation requires $p^* > \frac{1}{2}\max\{\lambda_2(L_A), \lambda_2(L_B)\}$ to hold. Here, we show this condition is feasible if algebraic connectivities of G_A and G_B are close to one another. First, if $\lambda_2(L_A) = \lambda_2(L_B)$ and $v_{2A} \neq v_{2B}$, then $p^* > \frac{1}{2}\max\{\lambda_2(L_A), \lambda_2(L_B)\}$, because according to inequality (10),

$$p^* > \frac{1}{\lambda_2^{-1}(L_A) + \lambda_2^{-1}(L_B)},$$

which holds for $v_{2A} \neq v_{2B}$. Therefore, if $\lambda_2(L_A) = \lambda_2(L_B)$ and $v_{2A} \neq v_{2B}$, then

$$p^* > \frac{1}{2}\lambda_2(L_A) = \frac{1}{2}\lambda_2(L_B) = \frac{1}{2}\max\{\lambda_2(L_A), \lambda_2(L_B)\}.$$

Having non-identical Fielder vectors v_{2A} and v_{2B} is crucial for achieving superdiffusion without structural transition. Indeed, if $v_{2A} = v_{2B}$ then it is never possible to have $p^* > \frac{1}{2}\max\{\lambda_2(L_A), \lambda_2(L_B)\}$, because in this case

$$p^* = \frac{1}{\lambda_2^{-1}(L_A) + \lambda_2^{-1}(L_B)} \leq \frac{1}{2}\max\{\lambda_2(L_A), \lambda_2(L_B)\}$$

with equality only if $\lambda_2(L_A) = \lambda_2(L_B)$.

The condition $\lambda_2(L_A) = \lambda_2(L_B)$ is not a necessary condition though, i.e., having $p^* > \frac{1}{2}\max\{\lambda_2(L_A), \lambda_2(L_B)\}$ is not limited to interconnected networks for which $\lambda_2(L_A) = \lambda_2(L_B)$. To show this, let us consider any two irreducible

adjacency matrices A and C, and define L_A and L_C as the Laplacian matrices, such that $\lambda_2(L_A) < \lambda_2(L_C)$ and $v_{2A} \neq v_{2C}$. We construct an interconnected network consisting of A and $B = \alpha C$, where $\alpha > 0$ is a positive scalar. For this interconnected network, the coupling threshold $p^*(\alpha)$ is a function of α. In order to have $p^*(\alpha) > \frac{1}{2}\max\{\lambda_2(L_A), \lambda_2(L_B)\}$, the function $f(\alpha)$ defined as

$$\begin{aligned} f(\alpha) &= p^*(\alpha) - \frac{1}{2}\max\{\lambda_2(L_A), \lambda_2(L_B)\} \\ &= p^*(\alpha) - \frac{1}{2}\max\{\lambda_2(L_A), \alpha\lambda_2(L_C)\}. \end{aligned}$$

must be positive. Since matrix B is only a scale of C, $v_{2B} = v_{2C}$, hence $v_{2A} \neq v_{2B}$. Also, for $\alpha = \frac{\lambda_2(L_A)}{\lambda_2(L_C)}$, $\lambda_2(L_B) = \lambda_2(\alpha L_C) = \alpha\lambda_2(L_C) = \lambda_2(L_A)$. Thus, according to our argument about the case where $\lambda_2(L_B) = \lambda_2(L_A)$, $f(\alpha = \lambda_2(L_A)/\lambda_2(L_C)) > 0$. Since $f(\alpha)$ is a continuous function of α, there exists ε, such that $f(\alpha) > 0$ for $\alpha \in \frac{\lambda_2(L_A)}{\lambda_2(L_C)}[1, 1+\varepsilon)$. Therefore, for $\lambda_2(L_B)/\lambda_2(L_A) \in [1, 1+\epsilon)$, $f(\alpha) > 0$, indicating that $p^* > \frac{1}{2}\max\{\lambda_2(L_A), \lambda_2(L_B)\}$.

The value of ϵ depends on the structure of A and C. However, we know that ϵ cannot be greater than 1. This comes from (11). If $\lambda_2(L_B) \geq 2\lambda_2(L_A)$, then

$$p^* \leq \min\{\lambda_2(L_A), \lambda_2(L_B)\} = \lambda_2(L_A) \leq \frac{1}{2}\lambda_2(L_B) = \frac{1}{2}\max\{\lambda_2(L_A), \lambda_2(L_B)\}.$$

Therefore, superdiffusion can be achieved without structural transition, but only if algebraic connectivities ofG_A and G_B are close to one another and their Fiedler vectors are not identical.

B.viii. Derivation of a Class of Upper Bounds with Explicit Interrelation Descriptors

Using formula (9), we derive a class of upper bounds $p^* \leq \frac{1}{\hat{\rho}_{n_A,n_B}}$ with the eigenvectors corresponding to the n_A smallest positive eigenvalue of L_A and the n_B smallest positive eigenvalue of L_B. The rationale for this upper bound is that

$$\begin{aligned} \rho(L_A^\dagger + L_B^\dagger) &= \rho\left(\sum_{i=2}^{N}\frac{1}{\lambda_i(L_A)}v_{Ai}v_{Ai}^T + \sum_{j=2}^{N}\frac{1}{\lambda_j(L_B)}v_{Bj}v_{Bj}^T\right) \\ &\geq \rho\left(\sum_{i=2}^{n_A+1}\frac{1}{\lambda_i(L_A)}v_{Ai}v_{Ai}^T + \sum_{j=2}^{n_B+1}\frac{1}{\lambda_j(L_B)}v_{Bj}v_{Bj}^T\right) \triangleq \hat{\rho}_{n_A,n_B}. \end{aligned} \tag{B.17}$$

Therefore $\frac{1}{\hat{\rho}_{n_A,n_B}}$ is an upper bound for $p^* = \frac{1}{\rho(L_A^\dagger + L_B^\dagger)}$.

The special structure of the matrix $\sum_{i=2}^{n_A+1}\frac{1}{\lambda_i(L_A)}v_{Ai}v_{Ai}^T + \sum_{j=2}^{n_B+1}\frac{1}{\lambda_j(L_B)}v_{Bj}v_{Bj}^T$ in (B.17) allows for a very efficient computation of $\hat{\rho}_{n_A,n_B}$.

Claim: For the upper bound $\frac{1}{\hat{\rho}_{n_A,n_B}}$, $\hat{\rho}_{n_A,n_B}$ can be computed as the spectral radius of an $(n_A+n_B)\times(n_A+n_B)$ matrix H, i.e.,

$$\hat{\rho}_{n_A,n_B} = \rho(H), \tag{B.18}$$

$$H \triangleq \left(u_{(n_A+n_B)}\begin{bmatrix}\boldsymbol{\lambda}^{-1}(L_A)\\ \boldsymbol{\lambda}^{-1}(L_B)\end{bmatrix}^T\right) \circ \begin{bmatrix} I_{n_A} & \boldsymbol{v}_A^T\boldsymbol{v}_B \\ \boldsymbol{v}_B^T\boldsymbol{v}_A & I_{n_B}\end{bmatrix}, \tag{B.19}$$

where $\circ$ denotes the Hadamard (entry-wise) product [6], $\boldsymbol{\lambda}^{-1}(L_A) \triangleq [\lambda_2^{-1}(L_A), \cdots, \lambda_{n_A+1}^{-1}(L_A)]^T$, $\boldsymbol{v}_A = [v_2(L_A), \cdots, v_{n_A+1}(L_A)] \in \mathbb{R}^{N\times n_A}$, and $\boldsymbol{\lambda}^{-1}(L_B)$ and $\boldsymbol{v}_B$ are defined similarly.

Proof: Suppose that μ is an eigenvalue of the matrix inside the parantethis in (B.17), i.e.,

$$\sum_{i=2}^{n_{A+1}}\frac{1}{\lambda_i(L_A)}v_i(L_A)v_i^T(L_A)x + \sum_{j=2}^{n_{B+1}}\frac{1}{\lambda_j(L_B)}v_j(L_B)v_j^T(L_B)x = \mu x. \tag{B.20}$$

Multiplying both sides of (B.20) by $v_k^T(L_A)$ and $v_h^T(L_B)$, for $k \in \{2, ..., n_A + 1\}$ and $h \in \{2, ..., n_B + 1\}$, and defining $\xi_i^A \triangleq v_i^T(L_A)x$, $\xi_j^B = v_j^T(L_B)x$, and $r_{ij} = r_{ji} = v_i^T(L_A)v_j(L_B)$, we obtain:

$$\frac{1}{\lambda_k(L_A)}\xi_k^A + \sum_{j=2}^{n_B+1} \frac{1}{\lambda_j(L_B)} r_{kj}\xi_j^B = \mu\xi_k^A, \tag{B.21}$$

$$\sum_{i=2}^{n_A+1} \frac{1}{\lambda_i(L_A)} r_{hi}\xi_i^A + \frac{1}{\lambda_h(L_B)}\xi_h^B = \mu\xi_h^B, \tag{B.22}$$

for $k \in \{2, ..., n_A + 1\}$ and $h \in \{2, ..., n_B + 1\}$. This equation can be written as

$$H \begin{bmatrix} \boldsymbol{\xi}^A \\ \boldsymbol{\xi}^B \end{bmatrix} = \mu \begin{bmatrix} \boldsymbol{\xi}^A \\ \boldsymbol{\xi}^B \end{bmatrix}, \tag{B.23}$$

where $\boldsymbol{\xi}^A \triangleq [\xi_2^A, ..., \xi_{n_A+1}^A]$ and $\boldsymbol{\xi}^B \triangleq [\xi_2^B, ..., \xi_{n_B+1}^B]$ and H is defined as (B.19). According the definition (B.17), $\hat{\rho}_{n_A,n_B}$ is the largest eigenvalue of H, therefore based on (9), $1/\rho(H)$ is an upper bound for p^*, proving the upper bound formula (B.18). □

The interesting aspect of the upper bound $p^* \leq \frac{1}{\hat{\rho}_{n_A,n_B}}$ is not only its dependence on the smallest positive eigenvalues of L_A and L_B, but also on the inner product of their corresponding eigenvectors, thus explicitly incorporating the network interrelation. By computing a few eigenvectors of L_A and L_B, this upper bound gives very good estimates with increasing precision as the number of eigenvectors n_A and n_B increases. The upper bound $p^* \leq \frac{1}{\hat{\rho}_{n_A,n_B}}$ is essentially different from (11), for it includes terms $v_A^T v_B$ denoting network interrelations, because the inner product of the eigenvectors changes if component G_B is reoriented with respect to G_A.

C. SOME NOTES ON NETWORK INTERRELATION

In the main text, we argued that the exact coupling threshold equation (8) depends, in a nonlinear way, on the matrices L_A, L_B, $\tilde{L}$, $\bar{L}$, and $\bar{L}^{\dagger}$ in Eq. (5-7), and unveils that the structural transition phenomenon is jointly caused by A and B. Considering the network G_A, G_B, or the superpositioned network G_s separately, can only partially characterize the structural transition phenomenon. The finer details, as (8) tells us, need all players collectively. These results highlight a more fundamental aspect of interconnected/multilayer networks: the information embedded in an interconnected network is more than the information embedded in graph properties of its components and their aggregates.

Any behavior of the interconnected network $\mathcal{G}(A, B)$ is due to the joint influence of A and B simultaneously. Therefore, a descriptor of this behavior must incorporate this joint influence. The challenge is that while network science and graph theory provide advanced and established tools to study G_A and G_B individually, not many results are known so far on how to characterize their joint effect. To the best of our knowledge, this concept is not yet thoroughly understood in the context of joint graph analysis, though other analogous concepts are very familiar. In multivariate probability theory, for example, we know that joint probability of a pair of random variables cannot be explained by their marginal probabilities. Similarly, the joint influence of network components cannot be explained in terms of graph properties of each component individually. In this line of analogy, as demonstrated in Table I, we can think of interrelation descriptors for interconnected/multilayer networks having the same role that correlation coefficient has for two random variables.

TABLE I: An analogy between interconnected/multilayer networks and multivariate probability.

Multilayer Network	**Multivariate Probability**
Multilayer network $\mathcal{G}(A, B)$	Joint distribution $f_{X,Y}(x, y)$
Graph layers G_A and G_B	Marginal distributions $f_X(x)$ and $f_Y(y)$
Graph properties of each layer	Statistics of each marginal distribution
Layers interrelation	Correlation between random variables
Interrelation descriptors	Correlation coefficient $r_{X,Y}$

Interrelation descriptors quantify how one network component is positioned with respect to the other. One example of interrelation descriptor is the node degree correlation across the two components $r(d_A, d_B)$. Whether high-degree nodes of G_A correspond to high-degree nodes of G_B can make a big difference on how the overall interconnected network behaves. For example, it was shown [7] that for spreading of two competitive viruses in a multilayer network, coexistence is more feasible if network layers have negative degree correlations, i.e, high-degree nodes of one layer have a low degree in the other layer and vice versa. Other researchers have pointed out the interrelation concept to some extent. For example, Lee *et al.* [8] studied how degree correlation of G_A and G_B impacts the size of the giant component in a percolation process. Juher and Saldaña [9] studied how to align network layers, each with a given degree distribution, to achieve maximal degree correlation. In our upper bound (B.18), we identified that the inner product of Fielder vectors of each component is a relevant interrelation descriptor for the structural transition phenomena, while the degree correlation between network components is not. For example, from Fig. 3 in the main text and Fig. 5 in this Supplemental Material, it follows that when Fielder vectors are almost orthogonal, i.e., $v_{2A}^T v_{2B}$ is small, the upper bound $\min\{\lambda_2(L_A), \lambda_2(L_B)\}$ is more accurate than $\frac{1}{2}\lambda_2(\bar{L})$. While when the two Fiedler vectors are almost aligned, i.e., $v_{2A}^T v_{2B}$ is large, then $\frac{1}{2}\lambda_2(\bar{L})$ becomes more accurate. Furthermore, in this case, the lower bound $1/(\lambda_2^{-1}(L_A) + \lambda_2^{-1}(L_B))$ in Eq. (10) becomes more accurate.

D. INTERCONNECTION OF MULTIPLE NETWORKS

We can extend our analysis to interconnection of multiple networks. As depicted in Figure 7, suppose m networks are coupled to each other. How these networks are connected to each other can be arbitrary. We can show this by a graph H, which we refer to as interconnection graph. Each node of this graph is a network and links of the graph indicate coupling between networks. For the case of $m = 2$ in the main manuscript, $H = \begin{bmatrix} 0 & 1 \\ 1 & 0 \end{bmatrix}$. For $m > 2$, H can be any arbitrary connected graph. Furthermore, between each two network G_k and G_j, the interconnection is determined by an $N-$by$-N$ matrix B. In the case of the one-to-one correspondence structure studied in the main text, i.e., node i in network G_k is connected to node i in network G_j, then B is equal to the identity matrix. With this setup, the adjacency and Laplacian matrices can be written as

$$\boldsymbol{A} = \bigoplus_{i=1}^{m} A_i + p(H \otimes B), \tag{D.1}$$

$$\boldsymbol{L} = \bigoplus_{i=1}^{m} L_i + p(L_H \otimes B), \tag{D.2}$$

where matrices A_i and L_i are the adjacency and Laplacian matrix of network i, respectively, and $\bigoplus$ denote matrix direct sum. For example, $\bigoplus_{i=1}^{m} A_i \triangleq diag(A_1, \ldots, A_m)$ is the block diagonal matrix with A_i matrices on its diagonal. Additionally, H and L_H are the $m \times m$ adjacency and Laplacian matrix, respectively, of the interconnection graph between the m networks. The matrix B specifies the same interconnection patterns between nodes in network G_k and G_j, and $\otimes$ is the matrix Kronecker product [4]. Therefore, $H \otimes B$ determines the overall interconnection pattern for a positive coupling weight $p > 0$.

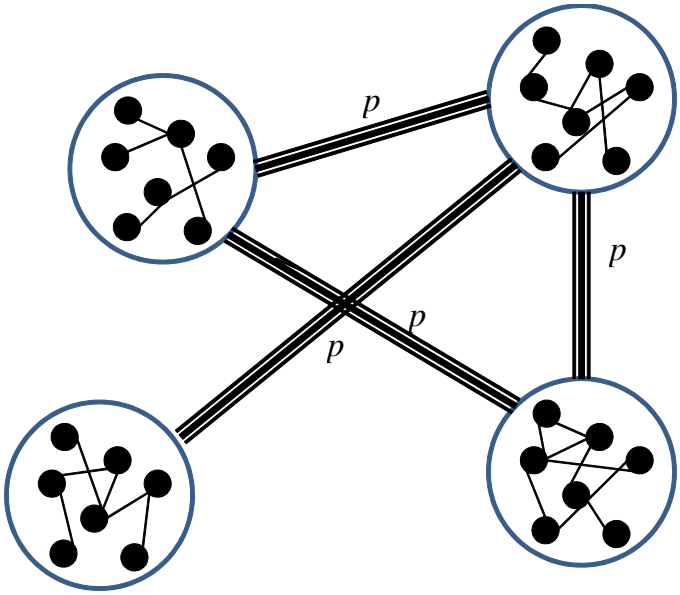

FIG. 7: Interconnection of multiple networks.

Claim: The eigenvalue equation of the $mN \times mN$ Laplacian matrix $\boldsymbol{L} = \bigoplus_{i=1}^{m} L_i + p(L_H \otimes B)$ of the interconnected network,

$$\boldsymbol{Lv} = \lambda \boldsymbol{v}, \tag{D.3}$$

has, besides the eigenvector $\boldsymbol{v} = \boldsymbol{u}$ corresponding to $\lambda = 0$, another set of solutions

$$\boldsymbol{v} = v_k(L_H) \otimes u, \tag{D.4}$$

$$\lambda = \lambda_k(L_H)\alpha p, \ k \in \{2, \ldots, m\}, \tag{D.5}$$

provided the all-one vector u is an eigenvector of the matrix B corresponding to the largest eigenvalue $\lambda_N(B) = \alpha$.

Proof: Right-multiplication of $\boldsymbol{L}$ by the $mN \times 1$ vector $\boldsymbol{w} = x \otimes u$ yields

$$\boldsymbol{L}\boldsymbol{w} = \bigoplus_{i=1}^{m} L_i \boldsymbol{w} + p(L_H \otimes B)(x \otimes u). \tag{D.6}$$

Invoking the mixed-product [4, p. 254] of the Kronecker product,

$$(A_1 \otimes B_1)(A_2 \otimes B_2) = (A_1 A_2) \otimes (B_1 B_2), \tag{D.7}$$

and the fact that for any Laplacian matrix L, it holds that $Lu = 0$, leads to

$$\boldsymbol{L}(x \otimes u) = p(L_H x) \otimes (Bu). \tag{D.8}$$

The right-hand side vector $\boldsymbol{v} = x \otimes u$ is an eigenvector of $\boldsymbol{L}$ provided that

$$p(L_H x) \otimes (Bu) = \lambda(x \otimes u), \tag{D.9}$$

which is equivalent to the condition that $\alpha p L_H x = \lambda x$ and $Bu = \alpha u$. Only if the matrix B has an eigenvector u, which must, by the Perron-Frobenius theorem correspond to the largest eigenvalue $\alpha = \lambda_N(B)$, the condition can be satisfied. The eigenvalue equation $\alpha p L_H x = \lambda x$ corresponding to $\lambda > 0$, has $m-1$ possible eigenvector solutions $v_k(L_H)$ belonging to eigenvalue $\lambda_k(L_H)$ of the matrix L_H. □

Any regular connectivity pattern in which the row sum of B is constant, leads to an eigenvector u for B. If the interconnected network consists of $m = 2$ networks, connected one-to-one so that $B = I$, then $L_H = \begin{pmatrix} 1 & -1 \\ -1 & 1 \end{pmatrix}$ with $\lambda_2(L_H) = 2$ so that $\lambda(\boldsymbol{L}) = 2p$ is an eigenvallue of $\boldsymbol{L}$.

Since we are here concerned with the smallest, non-zero eigenvalue of $\boldsymbol{L}$, we choose $\lambda_k(L_H)$ as small as possible but non-negative, thus $k = 2$. Similar to section B.i, the eigenderivative equation at $\lambda = \lambda_2(L_H)\alpha p$ and $\boldsymbol{v} = v_2(L_H) \otimes u$ becomes

$$\begin{bmatrix} \bigoplus_{i=1}^{m} L_i + p(L_H \otimes B) - \lambda_2(L_H)\alpha p(I_m \otimes I_N) & -v_2(L_H) \otimes u \\ -v_2^T(L_H) \otimes u^T & 0 \end{bmatrix} \begin{bmatrix} \frac{d\boldsymbol{v}}{dp} \\ \frac{d\lambda}{dp} \end{bmatrix} = \begin{bmatrix} -\lambda_2(H)\alpha(v_2(L_H) \otimes u) \\ 0 \end{bmatrix}. \tag{D.10}$$

The critical coupling weight p^* is the point where the eigenderivative equation does not have a unique solution. Hence, p^* must be the solution of the following generalized eigenvalue probelm

$$\begin{bmatrix} \bigoplus_{i=1}^{m} L_i & -v_2(L_H) \otimes u \\ -v_2^T(H) \otimes u^T & 0 \end{bmatrix} x = p^* \begin{bmatrix} \lambda_2(L_H)\alpha(I_m \otimes I_N) - (L_H \otimes B) & \mathbf{0} \\ \mathbf{0} & 0 \end{bmatrix} x. \tag{D.11}$$

The right-hand side matrix is block-diagonalizable using the following transformation,

$$T = \begin{bmatrix} T_H \otimes I_N & 0 \\ 0 & 1 \end{bmatrix}, \tag{D.12}$$

where T_H is the orthogonal matrix with the eigenvectors of L_H in its columns.

E. COMPLEMENTARY RESULTS

E.i. Upper Bound in terms of Dirichlet Energies

We showed in (8) that $p^* = \frac{1}{2}\lambda_2(Q)$, half of the smallest positive eigenvalue of $Q = \bar{L} - \tilde{L}\bar{L}^\dagger\tilde{L}$. According to min-max theorem for eigenvalues [4]

$$\lambda_2(Q) = \min_{\substack{\|x\|_2=1,\\ u^T x=0}} x^T \left(\bar{L} - \tilde{L}\bar{L}^\dagger\tilde{L}\right) x. \tag{E.1}$$

Any arbitrary choice of $x \perp u$ leads to an upper bound for p^*. Specifically, if we use the Fiedler vector of the superpositioned network, i.e. the eigenvector $v_2(\bar{L})$ corresponding to $\lambda_2(\bar{L})$, we obtain:

$$\begin{aligned}\lambda_2(Q) &\leq v_2^T \left(\bar{L} - \tilde{L}\bar{L}^\dagger\tilde{L}\right) v_2 \\ &= \lambda_2(\bar{L}) - \sum_{i=2}^{N} \frac{1}{\lambda_i}(v_2^T\tilde{L}v_i)^2.\end{aligned} \tag{E.2}$$

Equation (E.2) provides an upper bound for p^* improving the upper bound $\frac{1}{2}\lambda_2(\bar{L})$ of [10], because (E.2) always gives a tighter bound as $\lambda_i > 0$. Interestingly, not only the summation of graph related matrices of the two networks is important, their difference also plays a major role. To highlight this observation, we only consider the first term $i = 2$ in the summation in (E.2)

$$\begin{aligned}\lambda_2(Q) &\leq \lambda_2(\bar{L}) - \frac{1}{\lambda_2(\bar{L})}(v_2^T\tilde{L}v_2)^2 \\ &= \lambda_2(\bar{L})\left(1 - (\frac{v_2^T\tilde{L}v_2}{v_2^T\bar{L}v_2})^2\right).\end{aligned} \tag{E.3}$$

Using the definition $\tilde{L} = \frac{1}{2}(L_A - L_B)$, we find an alternative upper bound for the coupling threshold as

$$p^* \leq \frac{1}{2}\lambda_2(\bar{L})\left(1 - \left(\frac{\mathcal{E}_A(v_2) - \mathcal{E}_B(v_2)}{\mathcal{E}_A(v_2) + \mathcal{E}_B(v_2)}\right)^2\right), \tag{E.4}$$

where $\lambda_2(\bar{L})$ is half of the algebraic connectivity of the superpositioned network and $v_2(\bar{L})$ is its Fiedler vector [4]. Furthermore, $\mathcal{E}_A(v_2) \triangleq v_2^T L_A v_2$ and $\mathcal{E}_B(v_2) \triangleq v_2^T L_B v_2$ are Dirichlet energies [11]. For example, if we intereprete graph G_A as an electric circuit where links are resistors with unit resistance, then $\mathcal{E}_A(v_2) = v_2^T L_A v_2$ is the running power in the circuit if v_2 assigns a voltage to each node. Not only the upper bound (E.4) improves the upper bound $\frac{1}{2}\lambda_2(\bar{L})$ of [10], it explicitly depends on the interrelation of G_A and G_B.

E.ii. A Shur's Complement Approach to Finding p^*

Aside from the procedure in Section B.i, we can use Shur's complement formula [4] for determinants to find values of p such that W defined in (B.3) is singular. Computing determinant $\det W$ by Shur's complement formula

$$\det\begin{bmatrix} A & B \\ C & D \end{bmatrix} = \det A \det\left(D - CA^{-1}B\right) \tag{E.5}$$

results in

$$\det W = \det\left(L_A - pI\right) \det\left(\begin{bmatrix} L_B - pI & u \\ u^T & 0 \end{bmatrix} - \begin{bmatrix} pI \\ u^T \end{bmatrix}\left(L_A - pI\right)^{-1}\begin{bmatrix} pI & u \end{bmatrix}\right).$$

We first execute the last matrix product

$$\begin{bmatrix} pI \\ u^T \end{bmatrix}\left(L_A - pI\right)^{-1}\begin{bmatrix} pI & u \end{bmatrix} = \begin{bmatrix} p^2\left(L_A - pI\right)^{-1} & p\left(L_A - pI\right)^{-1}u \\ pu^T\left(L_A - pI\right)^{-1} & u^T\left(L_A - pI\right)^{-1}u \end{bmatrix}. \tag{E.6}$$

Since u is an eigenvector of $(L - pI)$ corresponding to eigenvalue $-p$, it is also an eigenvector of $(L - pI)^{-1}$ corresponding to eigenvalue $-\frac{1}{p}$. Therefore,

$$(L_A - pI)^{-1} u = -\frac{1}{p} u.$$

so that the matrix (E.6) simplifies to

$$\begin{bmatrix} pI \\ u^T \end{bmatrix} (L_A - pI)^{-1} \begin{bmatrix} pI & u \end{bmatrix} = \begin{bmatrix} p^2 (L_A - pI)^{-1} & -u \\ -u^T & -\frac{N}{p} \end{bmatrix},$$

and

$$\begin{aligned} \det W &= \det (L_A - pI) \det \left(\begin{bmatrix} L_B - pI & u \\ u^T & 0 \end{bmatrix} + \begin{bmatrix} -p^2 (L_A - pI)^{-1} & u \\ u^T & \frac{N}{p} \end{bmatrix} \right) \\ &= \det (L_A - pI) \det \begin{bmatrix} L_B - pI - p^2 (L_A - pI)^{-1} & 2u \\ 2u^T & \frac{N}{p} \end{bmatrix}. \end{aligned}$$

We now apply the variant [4] of (E.5)

$$\det \begin{bmatrix} A & B \\ C & D \end{bmatrix} = \det D \det \left(A - BD^{-1}C \right),$$

to the last block determinant,

$$\det \begin{pmatrix} L_B - pI - p^2 (L_A - pI)^{-1} & 2u \\ 2u^T & \frac{N}{p} \end{pmatrix} = \frac{N}{p} \det \left(L_B - pI - p^2 (L_A - pI)^{-1} - \frac{4p}{N} uu^T \right).$$

Therefore,

$$\det W = \frac{N}{p} \det (L_A - pI) \det \left(L_B - pI - p^2 (L_A - pI)^{-1} - \frac{4p}{N} uu^T \right),$$

which we can also write, using $\det (A) \det (B) = \det (AB)$ as

$$\begin{aligned} \det W &= \frac{N}{p} \det \left((L_A - pI)(L_B - pI) - p^2 (L_A - pI)(L_A - pI)^{-1} - \frac{4p}{N} (L_A - pI) uu^T \right) \\ &= \frac{N}{p} \det \left((L_A - pI)(L_B - pI) - p^2 I - \frac{4p}{N} ((L_A - pI) u) u^T \right) \\ &= \frac{N}{p} \det \left(L_A L_B - p (L_A + L_B) + \frac{4p^2}{N} uu^T \right). \end{aligned}$$

Having $\det W = 0$ requires that $\det Z_{AB} = 0$, where

$$Z_{AB} = L_A L_B - p (L_A + L_B) + \frac{4p^2}{N} uu^T.$$

Further, $\det Z_{AB} = 0$ is equivalent to the existence of an eigenvector y_{AB} of Z_{AB} belonging to a zero eigenvalue such that $Z_{AB} y_{AB} = 0$, hence,

$$L_A L_B y_{AB} = p (L_A + L_B) y_{AB} - p^2 \frac{4 \left(u^T y_{AB} \right)}{N} u. \tag{E.7}$$

For $p = 0$, $y_{AB} = u$ solve the equation. For any other $p \neq 0$, y_{AB} must be orthogonal[1] to u, i.e., $u^T y_{AB} = 0$, in which

---

[1] Multiplying (E.7) by u^T from left yields:

$$u^T L_A L_B y_{AB} = p u^T (L_A + L_B) y_{AB} - p^2 \frac{4 \left(u^T y_{AB} \right)}{N} (u^T u)$$

which leads to

$$0 = 0 - 4p^2 \left(u^T y_{AB} \right).$$

Since, $p \neq 0$, $u^T y_{AB} = 0$.

case (E.7) simplifies to

$$L_A L_B y_{AB} = p^* \left(L_A + L_B\right) y_{AB}. \tag{E.8}$$

Similarly, we must have

$$L_B L_A y_{BA} = p^* \left(L_A + L_B\right) y_{BA}. \tag{E.9}$$

In general, $L_A L_B \neq L_B L_A$, unless L_A and L_B commute. However, the above two equations are not contradicting. Indeed, due to symmetry of L_A and L_B, y_{AB} is the right generalized eigenvector of $L_B L_A$ while y_{BA} is its left generalized eigenvector. Equation (E.8) is a generalized eigenvalue problem with nonsymetric matrices which can be effectively solved using Lanczos-based methods [12].

The above formula for p^* is consistent with previous expressions. Indeed, since y_{AB} is orthogonal to u, we can multiply E.8 by $L_B^\dagger L_A^\dagger$ to get

$$\frac{1}{p^*} y_{AB} = \left(L_A^\dagger + L_B^\dagger\right) y_{AB},$$

which is consistent with our previous results for p^* as found in (9).

Apart from the upper bounds for p^*, deduced in previous sections from the matrix Q, we find from (E.8) (and similarly for the $L_B L_A$ case) after multiplying both sides with y_{AB}^T that

$$p^* = \frac{y_{AB}^T L_A L_B y_{AB}}{y_{AB}^T \left(L_A + L_B\right) y_{AB}}. \tag{E.10}$$

Equation (E.10) expresses the coupling threshold p^* as an optimization problem for the vector y_{AB}, orthogonal to the vector u, and bears resemblance with the Rayleigh inequalities [4] for eigenvalues of a matrix. A lower bound follows from (E.10) for any non-zero vector $y \perp u$ as

$$p^* \geq \frac{\min_{y \neq 0 \text{ and } y^T u = 0} y^T L_A L_B y}{\max_{y \neq 0} y^T \left(L_A + L_B\right) y}.$$

* Electronic address: faryad@ksu.edu

[1] W. W. Zachary, J. Anthropol. Res. pp. 452–473 (1977).
[2] R. B. Nelson, AIAA journal **14**, 1201 (1976).
[3] W. C. Mills-Curran, AIAA journal **26**, 867 (1988).
[4] P. Van Mieghem, *Graph Spectra for Complex Networks* (Cambridge Univ Pr, 2011).
[5] S. Gómez, A. Diaz-Guilera, J. Gómez-Gardeñes, C. J. Pérez-Vicente, Y. Moreno, and A. Arenas, Phys. Rev. Lett. **110**, 028701 (2013).
[6] C. R. Johnson, *Matrix theory and applications* (American Mathematical Soc., 1990).
[7] F. D. Sahneh and C. Scoglio, Physical Review E **89**, 062817 (2014).
[8] K.-M. Lee, J. Y. Kim, W.-k. Cho, K. Goh, and I. Kim, New Journal of Physics **14**, 033027 (2012).
[9] D. Juher and J. Saldaña, arXiv preprint arXiv:1504.02031 (2015).
[10] F. Radicchi and A. Arenas, Nat. Phys. **9**, 717 (2013).
[11] P. E. Jorgensen and E. P. J. Pearse, Comp. Anal. Oper. Theor. **4**, 975 (2010).
[12] C. Rajakumar and C. Rogers, International Journal for Numerical Methods in Engineering **32**, 1009 (1991).